93-332

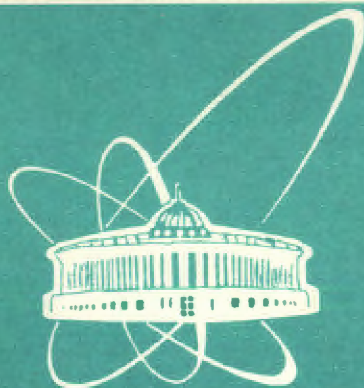

сообщения
объединенного
института
ядерных
исследований
дубна

E9-93-332

J.Pivarč*

MAIN FEATURES OF ECR ION SOURCE VACUUM SYSTEMS

*Home address: Institute of Physics, Slovak Academy of Sciences, Dúbravska cesta 9, 842 28 Bratislava, Slovakia

1993

I.INTRODUCTION

At the Flerov Laboratory of Nuclear Reactions in Dubna (Russia) the ECR ion source DECRIS (Dubna Electron Cyclotron Ion Source) is being built[1]. It will be used to all fields of science using multiple charge heavy ions[2].

The vacuum system of an ECR ion source is one of the main components of the source. Whereas, operating pressure ranges for vacuum systems of the accelerators are 10^{-4} - 10^{-9} Pa [3], the required operating pressure range for the vacuum system of the ECR ion source is 10^{-2} - 10^{-5} Pa, respectively. Basically, it consists of stainless steel, copper beam tubes pumped with turbomolecular, cryosorption, getter - Ti - sublimation, NEG pumps combined with sorption and rotary pumps. The combination of turbomolecular and rotary pumps is being used for the time in the DECRIS ion source. Other suitable combinations of vacuum pumps as well as the pressure measuring gauges are shown in Fig. 1.

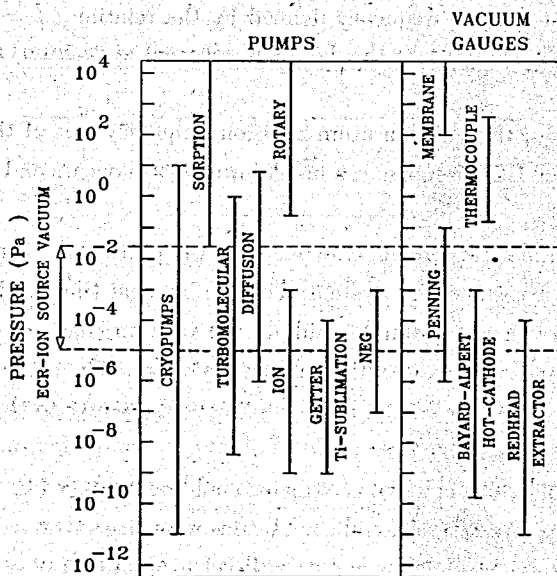

Fig. 1. Vacuum pumps and gauges used for pumping and pressure measurement in ECR ion sources.

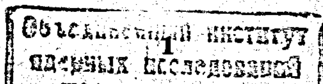

This paper reports in detail sequences of the vacuum system design of the ECR ion source as well as molecular conductance, beam pipe outgassing and gas desorption processes (ion induced pressure instability, hydrogen diffusion and desorption) and influence of neutral gases on the operated vacuum inside the beam pipe of the ion source.

II.ECR ION SOURCE GENERAL LAYOUT

In the ECR concept[4–5] low pressure gas is heated by microwaves which accelerate also the ionizing electrons within the Ioffe magnetic trap. The source consists minimally of two axisymmetric coils with a hexapole between them. Therefore, a plasma with hot electrons and cold ions is formed. The microwave frequency ω must match the cyclotron frequency $\omega_c = e|B(x)|/m_e$ (e is the electron charge, B is the magnetic induction in side the plasma and m_e is the electron mass) on a closed heated surface called the ECR surface. However, there also exists a plasma density effect which shifts the resonance frequency ω_c from the ECR resonance towards upper (ω_H) and low (ω_L) hybrid resonances. These new resonances occur at higher and weaker magnetic fields and their frequences are given by the formulas

$$\omega_H^2 = \omega_p^2 + \omega_c^2, \qquad \omega_L^2 = \frac{m_e}{m_i}(\omega_p^2 + \frac{m_e}{m_i}\omega_c^2)$$

where ω_p is the plasma frequency defined by the relation $\omega_p^2 = n_e e^2/\epsilon_o m_e$ (n_e is the electron density and ϵ_o is the dielectric constant of vacuum) and m_i is the ion mass[6].

If, in addition, the electron atom collision frequency ν is of the same order or smaller than the ECR frequency, a breakdown always occurs and the ECR plasma is ignited[4].

The ion charge state q strongly depends on the particle life-time which depends on the magnetic confinement system. The confinement time is of the order of ms.

The plasma is heated from any side of the vacuum chamber of the ion source and it is also transparent to microwaves everywhere. Than, the plasma chamber behaves as a multimode cavity. The coupling of the power to the plasma deteriorates when ratio ω_p/ω increases.

Originally, only ions of gaseous elements could be produced by ECR ion sources, however, lately, a variety of metalic ion beams were also extracted and accelerated. For the metal ion production one uses direct evaporation of a sample by direct plasma impact or an oven for the sublimation of higher vapour pressure metals[7].

III.VACUUM SYSTEM DESIGN

The highest obtainable average pumping speed of the ECR ion source vacuum system strongly depends on the beam pump conductance. To illustrate this important limitation caused by the finite conductance, let us consider the system shown in Fig. 2. In the molecular flow regime the flow of molecules along the vacuum pipe to the nearest pump is expressed by the equation

$$Q(x) = -w\frac{dp}{dx} \qquad \frac{dQ}{dx} = Aq \tag{1}$$

where Q is the gas flow (Pa l s^{-1}), w is the specific molecular conductance (m l s^{-1}) (w = LC), C is the conductivity (l s^{-1}), p is the pressure inside the pipe (Pa), A is the specific surface area (cm^2 m^{-1}) (A = F/L), F is the surface area (cm^2) and q is the specific outgassing rate (uniform) (Pa l s^{-1} cm^{-2}). These equations can be combined to give

$$w\frac{d^2p}{dx^2} = -Aq \tag{2}$$

together with the boundary conditions of this simple problem

$$\left.\frac{dp}{dx}\right|_{x=L/2} = 0 \quad \text{and} \quad p|_{x=0} = \frac{AqL}{S} \tag{3}$$

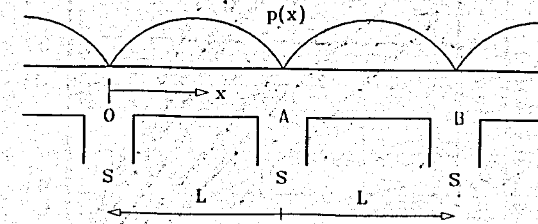

Fig. 2. Outline of the ECR pumping system. S is the pumping speed of the pump in points "O", "A", "B" (l s^{-1}), L is the distance between pumps (m) and x is the distance measured from the reference point "O" (m).

which follow from evident symmetry considerations. As the solution we can find a well known parabolic pressure profile along the beam pipe

$$p(x) = Aq\left(\frac{Lx - x^2}{2w} + \frac{L}{S}\right). \tag{4}$$

The maximum pressure occurs at the midpoint between pumps

$$p_{max} = Aq\left(\frac{L^2}{8w} + \frac{L}{S}\right). \tag{5}$$

For the ion source pipe the average pressure is more relevant

$$p_{av} = \frac{1}{L}\int_0^L p(x)dx = Aq\left(\frac{L^2}{12w} + \frac{L}{S}\right). \tag{6}$$

It is convenient to define an "effective linear pumping speed"

$$S_{eff} = \left(\frac{L^2}{12w} + \frac{L}{S}\right)^{-1} \tag{7}$$

so that $p_{av} = Aq/S_{eff}$. It is evident that S_{eff} cannot exceed $12w/L^2$ irrespective of how large pumps are used.

Equally, the lowest achievable average pressure is limited to $AqL^2/12w$. Since the conductance is generally determined by the appertures in electrodes and screens (screening of the high frequency), the only parameter is the interpump distance L. Obviously, many small pumps at short distance are preferable to few and large pumps. Fig. 3 illustrates this effect for a vacuum beam pipe conductance of 70

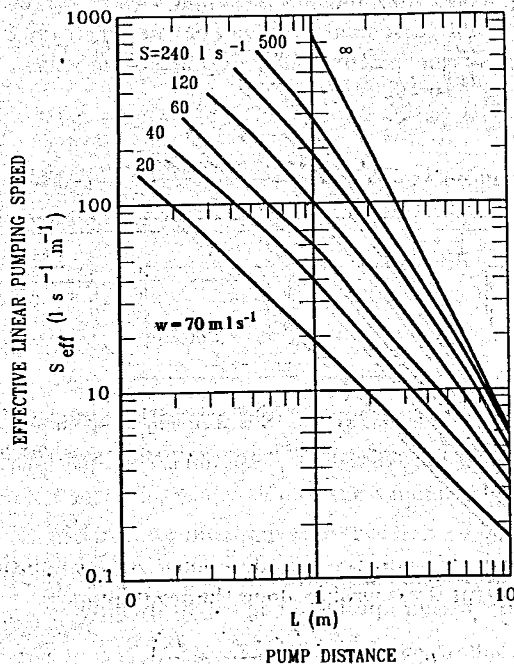

Fig. 3. Effective linear pumping speed S_{eff} as a function of pump distance L for various sizes of pumps, a vacuum beam pipe conductance w = 70 m l s^{-1} and different pumping speeds S = 20, 40, 60, 120, 240, 500 and ∞ l s^{-1}, respectively.

m l s^{-1} and different pumping speeds S (20, 40, 60, 120, 240, 500, ∞ l s^{-1}), respectively. It is shown that the effective pumping speed is practically the "linear" function of the pump distance for various sizes of pumps. Such a pumping structure may be installed along the vacuum system and hence the analysis provides a "linear pumping speed" inside the beam pipe.

The real pressure distribution and therefore the average pressure also follow from the equation similar to the previous one

$$-w\frac{d^2p}{dx^2} = Aq - sp \tag{8}$$

where s is the specific pumping speed defined as $s = S/L$ (l s^{-1} m^{-1}). By the solution of the differential equation (8) using the boundary conditions (3) we find other pressure profiles along the beam pipe. It holds that

$$p(x) = C_1e^{rx} + C_2e^{-rx} + \frac{Aq}{s} \tag{9}$$

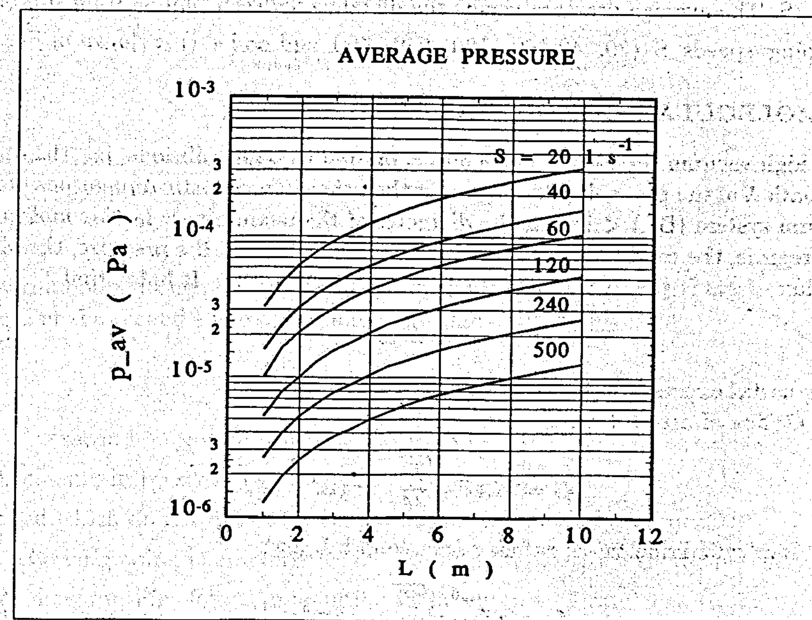

Fig. 4. Plot of the average pressure p_{av} versus distance L between pumps for different pumping speeds S = 20, 40, 60, 120, 240, 500 and ∞ l s^{-1}, respectively.

where

$$C_1 = \frac{AqL}{S}e^{-rL}(1+e^{-rL})^{-1}, \quad r = (s/w)^{0.5}$$

and

$$C_2 = \frac{AqL}{S}(1+e^{-rL})^{-1}.$$

Usually, the vacuum system is designed with respect to s≪w. In this configuration one can obtain

$$C_1 \cong C_2 \cong C_o = \frac{Aq}{2}\frac{L}{S}. \quad (10)$$

The equation (9) is reduced to

$$p(x) = C_o(e^{rx} + e^{-rx}) + \frac{Aq}{s} \quad (11)$$

and the average pressure is determined by

$$p_{av} = \frac{C_o}{rL}(e^{rL} - e^{-rL}) + \frac{Aq}{s} \cong \frac{2AqL}{S}. \quad (12)$$

It is evident that the lowest achievable pressure only depends on the ratio of 2AqL/S. The average pressure versus the distance between pumps L for different pumping speeds S (20, 40, 60, 120, 240, 500 and ∞ l s^{-1}) is shown in Fig. 4.

IV.MOLECULAR CONDUCTANCE

In high vacuum the flow of molecules is limited by wall collisions, i.e. the mean free path λ of the gas molecules is greater than the characteristic dimensions of the vacuum system ($D/\lambda < 1$; D is the diameter of the beam pipe). In this molecular flow regime, the conductance C (m^3 s^{-1}) is independent on the pressure, therefore the flux of gas is proportional to the pressure gradient Δp. It holds that

$$Q = C\,\Delta p. \quad (13)$$

Some useful expressions for conductance are[3,8]:

a) Orifice of area F (cm^2);

$$C = 36.4F\sqrt{\frac{T}{M}} \quad (m^3\ s^{-1}), \quad (14)$$

b) long cylindrical tube, radius r (m), length L (m);

$$C = 305\frac{r^3}{L}\sqrt{\frac{T}{M}} \quad (m^3\ s^{-1}) \quad (15)$$

c) long tube with elliptic section (semi-axes a, b), a (m), b (m);

$$C = 431\frac{a^2b^2}{L(a^2+b^2)^{1/2}}\sqrt{\frac{T}{M}} \quad (m^3\ s^{-1}) \quad (16)$$

where T is the absolute temperature (K) and M are the molecular weight.

The molecular flow through complex systems can be computed with Monte Carlo programs adapted to the specific geometry.

V.OUTGASSING OF THE BEAM PIPE

For every vacuum system the size of the required pumps is directly related to the outgassing. The first important source is the static and thermal outgassing of weakly adsorbed molecules and diffusion of H_2 from the bulk of the material. The standard procedure to reduce the thermal outgassing is the well known bakeout of the beam pipe. The pressure inside an unbaked system is mainly determined by water vapours. In a clean and well baked system H_2 will be the dominant residual gas constituent. Typically, total specific outgassing rate q for unbaked and baked beam pipe made of stainless steel is given in Table I. Therefore, the

Table I. Total specific outgassing rate q for unbaked and baked beam pipe made of stainless steel[3].

Process	Temperature (K)	q (Pa l s^{-1} cm^{-2})
unbaked 100 h pumpdown	293	10^{-7}
baked 30 - 150 h at 300 °C	573	10^{-10}

thermal outgassing rate dQ_T/dt of the surface area F = 1000 cm^2 (F is the surface area of the second stage of the ion source DECRIS) is given by

$$\frac{dQ_T}{dt} = Fq = 1\text{x}10^{-4}\ \text{Pa l s}^{-1}. \quad (17)$$

The second important source of gas in the ion source is the so called "dynamic" outgassing in presence of the beam. Here, strongly bound molecules can be desorbed which do not otherwise contribute to the thermal desorption.

The outgassing characteristics of several materials used in vacuum technology are shown in Fig. 5 [9]. The quantity of the outgassing rate very strongly depends on the finished treatment with materials (untreated; degreased: solvent, vapour; polished: mechanical, chemical, blast, electro; baked: non - metals at 80 - 100 °C up to 24 h, metals at 300 - 400 °C up to 100 h). It is also shown that the best metals used in the vacuum technology are Al, Cu and stainless steel. Then, in order to obtain the outgassing rate less than 10^{-8} Pa l s^{-1} cm^{-2} the vacuum systems are not using rubber, polyamids, epoxy, viton and PTFE materials, respectively.

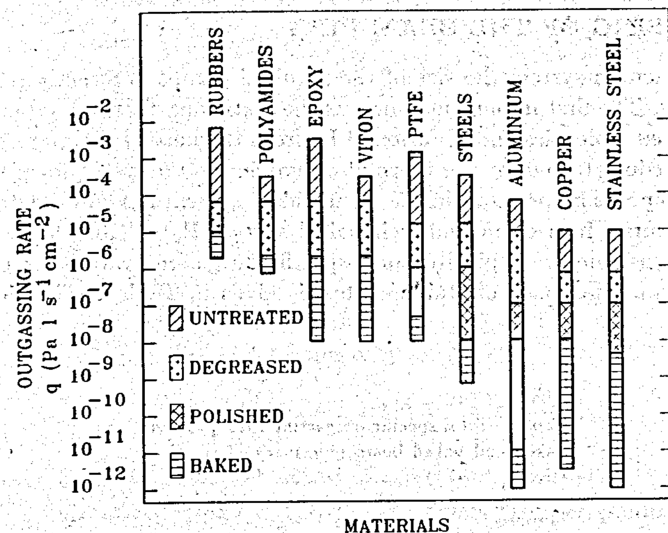

Fig. 5. Outgassing characteristics of several materials used in vacuum technology[9].

The outgassing characteristics of materials exposed to vacuum are also published in papers[10–12].

VI.DESORPTION OF GASES

The pressure of 10^{-5} Pa must be maintained inside the ECR ion source and its beam pipe despite of:

- The thermal outgassing of surfaces;
- Outgassing due to the desorption of weakly bound molecules on the walls of the vacuum system;
- The ions induced by extracted and accelerated ions;
- The diffusion of hydrogen from the walls of the vacuum system;
- The neutral gas produced inside the plasma of the ECR ion source;
- The desorption of molecules generated by roentgen radiation.

There are also observed direct thermal effects produced by the radiation. The radiation is also penetrating to the region of the beam pipe through the orifices in the anode and the extraction system of the source. Therefore, even water cooling parts of the first and second stages and other small areas of the source,

as for example the input flange of the high frequency generator, can be above the ambient temperature by 80 °C or more with a corresponding increase in their thermal outgassing rate by an order of magnitude or more[12–13]. To establish the given pressure for the given pumping speed the average thermal outgassing rate and the total average desorption rate must be below certain definite values.

A.Ion - induced pressure instability

The ions induced by extracted and accelerated beam can produce desorption of strongly bound molecules. The desorption flow rate n_i, Q_i can be expressed by[3,14]

$$n_i = \eta\sigma L(I/e)n \qquad Q_i = \eta\sigma L(I/e)p \tag{18}$$

where η is the molecular desorption yield (molecules ion^{-1}), σ is the ionization cross section of extracted and accelerated ions (m^2) (for example for high energy protons $\sigma = 1.2 \times 10^{-22}$ m^2 and for CO [3]), L is the length of beam section (m), I is the beam intensity (A), e is the electron charge (A s), n is the number of molecules in unit volume (m^{-3}) and p is the pressure (Pa). Note, if ions are taken from the restgas, then η will represent a net desorption yield. For $\eta < 0$ "a beam pumping" can be observed, i.e. the system acts like an ion pump. In the presence of the ion induced desorption $\eta > 0$ and the equilibrium pressure can be expressed as

$$p = Q/S_{eff} = \frac{\eta\sigma(I/e)p + qA}{S_{eff}} \tag{19}$$

which gives

$$p(I) = \frac{p_o}{1 - \frac{\sigma}{e}\frac{\eta I}{S_{eff}}} \tag{20}$$

where $p_o = q\,A/S_{eff}$.
By introducing

$$(\eta I)_{crit.} = \frac{e}{\sigma}S_{eff} \tag{21}$$

we obtain

$$p = \frac{p_o}{1 - \frac{\eta I}{(\eta I)_{crit.}}}. \tag{22}$$

Hence, the "critical current" product for $S \longrightarrow \infty$ cannot exceed

$$(\eta I)_{crit.} = \frac{e}{\sigma}\frac{12w}{L^2}. \tag{23}$$

Therefore, the pressure p is a function of the beam current I. The higher is the current I, the higher is the equilibrium pressure p.

The conductance of the beam pipe and the pump distance are also crucial parameters for vacuum stability. The remedy "defect" caused by the pressure bumps in the vacuum system of the source can be reduced by adding cryogenic, getter - Ti sublimation, or NEG pumps, respectively[15–16]. By 300 °C bakeout and Ar glow discharge cleaning of the source stages and beam pipes we can also reduce

the molecular desorption yield η. The glow discharge cleaning could be done as shown in Fig. 6.

By the way, the required ion doze on the beam pipe is typically 10^{18} cm^{-2} and results in that $\eta \leq 0^3$. The Ar glow discharge gives efficient sputtering and desorption of strongly adsorbed gas molecules. On the other hand, the addition of O_2 produces from carbon contaminants on the surface CO and CO_2 compounds which can easily be pumped out.

However, the ion - induced pressure instability desorption rate dQ_i/dt is given by

$$\frac{dQ_i}{dt} = 10^3 Q_i \cong 3\text{x}10^{-7}\ \text{Pa l s}^{-1} \tag{24}$$

if the molecular desorption rate $\eta = 1$ molecules ion^{-1}, the length $L = 0.45$ m, the beam current $I = 10^{-3}$ A, and the pressure $p = 10^{-3}$ Pa, respectively.

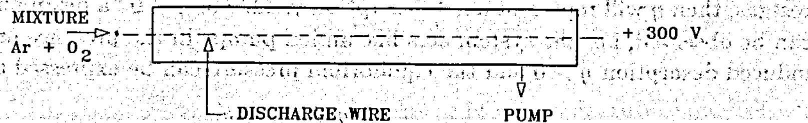

Fig. 6. Layout of the glow discharge cleaning.

B.Hydrogen diffusion and desorption

To describe the dependence of the hydrogen desorption rate on the exposure of photons and electrons it was assumed that the desorbing hydrogen is first transported by a diffusion process to the surface. Neglecting chemical reactions on the surface, a simplification which appears to be justified in the case of hydrogen, the gas - solid interaction may be characterized by both volume (diffusion) and surface processes (adsorption, desorption)[17]. In a simplified, one dimensional model of diffusion, the transport of molecules inside the bulk may be described by

$$\frac{\partial c}{\partial t} = D\frac{\partial^2 c}{\partial x^2}, \quad R = Kc \tag{25}$$

where c is the gas concentration inside the solid (cm^3 (STP) cm^{-3}). Because of the long term heat and vacuum treatment c is assumed to be in balance with the surface region. K is the phenomenological constant depending on irradiation current, photon energy spectrum and cross section for desorption ($cm\ s^{-1}$), D is the diffusion coefficient in the solid ($cm^2\ s^{-1}$) and R is desorbed gas flux (cm^3 (STP) $s^{-1}cm^{-2}$). Further the re-absorption is neglected because of high pumping

speed and low absorption coefficient for hydrogen in Al and stainless steel[8]. So, the net gas flux R leaving the surface is given by

$$R_o = -D\frac{\partial c}{\partial x}\bigg|_{x=0} = Kc|_{x=0}. \tag{26}$$

An analytical solution of equation (25) with the boundary condition (26) and with an uniform concentration c_o inside the bulk as a starting condition for a semi - infinite plate is[18]

$$R = R_o(t=0)\ e^{\tau}[1 - erf(\frac{1}{\sqrt{\tau}})] \tag{27}$$

where $\tau = \frac{K^2}{D}t$ and

$$erf(\frac{1}{\sqrt{\tau}}) = \frac{2}{\sqrt{\pi}}\int_0^{\frac{1}{\sqrt{\tau}}} e^{-u^2}du \quad \text{and}$$

$$\lim_{\tau \to 0+}\int_0^{\frac{1}{\sqrt{\tau}}} e^{-u^2}du = \frac{\sqrt{\pi}}{2}.$$

From this solution follows that R decreases after an initial time t_o according $1/\sqrt{t}$. This model has been used[17] in order to describe the measured data for different samples (AlMgSi, Al_2O_3, a high temperature steel type "NIMONIC"). The normalized desorption flux log (R/R_o) has been expressed as a function of the normalized time log τ in Fig. 7 for the photon (PSD) and electron (ESD) stimulated desorption. Then, it holds that the desorbed hydrogen flux R can be expressed for $\log(R/R_o) = 0$ and $\log(\frac{K^2}{D}t) \leq -2$ by

$$R_{PSD} = 0.0316c_o(\frac{D_{PSD}}{t})^{1/2} \tag{28}$$

$$R_{ESD} = 0.00316c_o(\frac{D_{ESD}}{t})^{1/2} \tag{29}$$

The normalized desorption fluxes log (R/R_o) can be described by

$$log(R/R_o)_{PSD} = -0.5log\ \tau - 0.833 \tag{30}$$

$$log(R/R_o)_{ESD} = -0.5log\ \tau - 2.833 \tag{31}$$

if $\log \tau \geq 0$.

Table II and Table III give a summary of the parameters D, c_o, η, ρ and R for all investigated samples[17].

This one dimensional diffusion model doesn't describe several effects observed during photon bombardment experiments, e.g. non - linearity with radiation intensity, recontamination during an interruption of the photon exposure "beam stop".

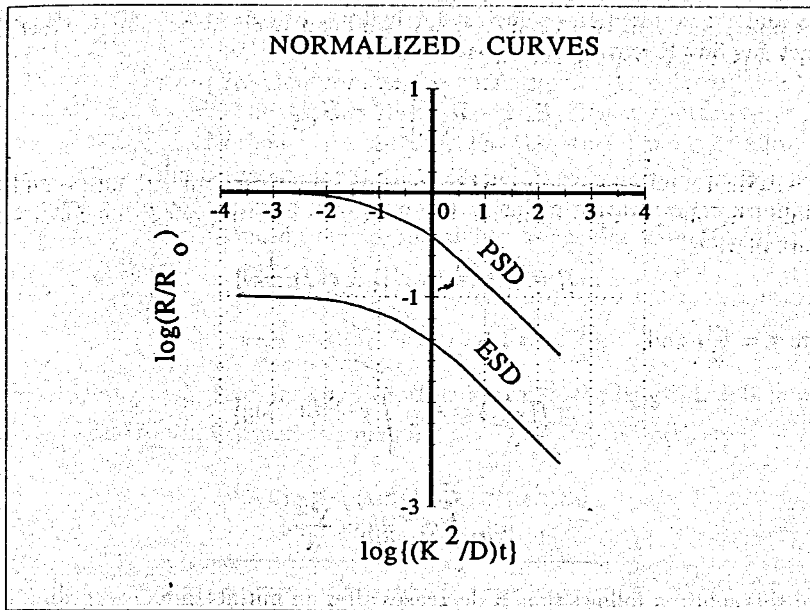

Fig. 7. Normalized hydrogen desorption flux log (R/R_o) vs log τ ($\tau = \frac{K^2}{D}t$). The curve PSD corresponds to hydrogen desoption flux data obtained for photon irradiation samples and curve ESD for samples submitted by electron bombardment[17]. The mean deviation between the experimental and theoretical values was simulated by equation (27) and is ≤ 5 %.

The specific gas desorption rate caused by the roentgen radiation dq^r/dt can be calculated by equation

$$\frac{dq^r_{H_2}}{dt}(log\tau \leq -2) = R_{PSD}$$

or

$$R_{PSD} = 7\text{x}10^{-8} \text{ Pa l s}^{-1} \text{ cm}^{-2}.$$

Therefore, the gas desorption rate caused by the roentgen radiation $dQ^r_{H_2}/dt$ is given by

$$\frac{dQ^r_{H_2}}{dt}(log\tau \leq -2) = 7\text{x}10^{-5} \text{ Pa l s}^{-1}. \quad (32)$$

This can be the real contribution of the dynamic background to the total flow of desorbed H_2 molecules from the plasma source pipe which is caused by the roentgen radiation. Approximately the same contribution can be expected from

Table II. Parameters characterizing the hydrogen diffusion and the photon stimulated desorption (PSD) of hydrogen[17]. The critical energy of photons spectrum was $\epsilon_c = 773$ eV. The desorbed gas flux R_{PSD} was calculated by (28) for t = 1 h. The data were measured at the temperature T = 20 °C.

Sample	D_{PSD} (cm^2 s^{-1})	c_o (cm^3(STP) cm^{-3})	R_{PSD} (cm^3(STP) s^{-1} cm^{-2})	η (mol ph^{-1})	ρ (phe ph^{-1})
AlMgSi	1.5x10^{-18}	1.1x10^3	7.1x10^{-10}	1.9x10^{-3}	5.5x10^{-2}
Al_2O_3	8.7x10^{-19}	1.1x10^3	5.4x10^{-10}	2.0x10^{-3}	
NIMONIC STEEL	2.5x10^{-19}	1.1x10^3	2.9x10^{-10}	1.2x10^{-3}	2.8x10^{-2}

Table III. Parameters characterizing the hydrogen diffusion and the electron stimulated desorption (ESD) of hydrogen[17]. The bombarding electron energy was E_e = 300 eV. The desorbed gas flux R_{ESD} was calculated by (29) for t = 1 h. The data were measured at the temperature T = 35 °C.

Sample	D_{ESD} (cm^2 s^{-1})	c_o (cm^3(STP) cm^{-3})	R_{ESD} (cm^3(STP) s^{-1} cm^{-2})	η (mol ph^{-1})
AlMgSi	6.3x10^{-18}	1.1x10^3	1.5x10^{-9}	1.0x10^{-1}
NIMONIC STEEL	7.0x10^{-18}	1.1x10^3	1.5x10^{-9}	6.2x10^{-1}

other gases such as CO_2, CO, CH_4, etc. So, the total gas desorption rate caused by the roentgen radiation dQ^r/dt is given by the equation

$$\frac{dQ^r_i}{dt} = \sum_i \frac{dQ^r_i}{dt} \quad (33)$$

where dQ^r_i/dt is a desorption rate for an "i" gas.

VII.NEUTRAL GASES

The neutral gases can arise for example by recombinations of ions with electrons. The efficiency of the process is very high at the low energy of electrons and sufficiently long time of interactions of produced ions with electrons. At a low electron temperature the neutral gases strongly influence the balance of the plasma which is created from charge particles.

The ion - loss rate due to the recombination process can be described by the following equation[19]

$$\left(\frac{\partial n^+}{\partial t}\right) = -\alpha(n^+)^2 \quad (34)$$

where n^+ is the concentration of ions (cm^{-3}), t is the time (s) and α is the coefficient of recombination (cm^3 s^{-1}). The cofficient α may be approximated by

$$\alpha \cong \frac{10^{-13}}{\sqrt{T_e}} \quad (35)$$

where T_e is the temperature of electrons in the plasma (eV). For the typical values

reached in the ECR ion source $n^+ \cong 5\text{x}10^{10}$ cm^{-3} [20], $T_e \cong 5000$ eV [4], $\alpha \cong 1.4\text{x}10^{-15}$ cm^3 s^{-1}, and at the volume of the second stage of the ECR ion source of 1500 cm^3 (DECRIS), the corresponding neutral gas rate dQ_1^{ng}/dt will be given by

$$\frac{dQ_1^{ng}}{dt} \leq 2\text{x}10^{-8} \text{ Pa l s}^{-1}. \qquad (36)$$

The neutral gas is also generated as a residual gas from the usage gas flow rate. The usage rate for the solid and gas materials is varied depending on a variety of parameters. It has generally been confirmed by most of tests that the usage rates for many solid materials are approximately 1 mg h^{-1} [21]. It corresponds to consumption of

$$\frac{dQ_2^{ng}}{dt} = 2.5\text{x}10^{-3} \text{ Pa l s}^{-1}. \qquad (37)$$

The lowest usage rate has been obtained 0.1 mg h^{-1} for a calcium run. The usage rates for gaseous materials are approximately 0.06 cm^3(STP) min^{-1} [22]. It corresponds to a maximum consumption of

$$\frac{dQ_3^{ng}}{dt} = 0.1 \text{ Pa l s}^{-1}. \qquad (38)$$

So, the total neutral gas dQ_t^{ng}/dt for the gaseous materials operation is given by

$$\frac{dQ_t^{ng}}{dt} \leq \frac{dQ_1^{ng}}{dt} + \frac{dQ_3^{ng}}{dt} \cong 0.1 \text{Pa l s}^{-1}. \qquad (39)$$

In order to obtain suitable operation vacuum inside the beam pipe of the ion source of 10^{-4} Pa the effective pumping speeds for the solid material (S^s_{eff}) and the gaseous (S^g_{eff}) operations have to be related by

$$S^s_{\text{eff}} \cong 25 \text{ l s}^{-1} \quad \text{and} \quad S^g_{\text{eff}} \cong 1000 \text{ l s}^{-1},$$

respectively.

VIII.CONCLUSION

The present work describes not only the vacuum system design of the ECR ion sources but also provides the main predictions in the area of the thermal outgassing rate, the gas desorption rates caused by the ion - induced and the photon - induced diffusion desorptions and the neutral gas rates for the gaseous and the solid material operations. Taken together, all these data show that it may be impossible to obtain the suitable operation vacuum (10^{-4} Pa) inside the second stage of the ion source if the effective pumping speeds for the solid material operation $S^s_{eff} < 25$ l s^{-1} and the gaseous material operation $S^g_{eff} < 1000$ l s^{-1}, respectively.

In practice, it is very difficult to construct very effective, reliable and cheap vacuum system for an ECR ion source. The vacuum system of the source has to be designed with respect to obtaining the vacuum of 10^{-5} Pa, for about 10 h with a leak rate lower than 10^{-3} Pa l s^{-1} and the outgassing rate of the vacuum exposed surfaces lower than 10^{-7} Pa l s^{-1} cm^{-2}. The plasma tubes and beam tubes must be made of stainless steel, steel with stable structure and with a low relative magnetic permeability. The aluminium and copper can also be successfully used because of good mechanical properties, availability and very low desorption rates.

As, it is practically impossible to separate the effects of diffusion, outgassing, and permeation which are manifold higher in polymers than in metals[23], it is not recommended to use polymers for clean interior surfaces of the ECR ion source vacuum system.

Acknowledgements. The author gratefully acknowledges the support of the FLNR (Grant No.5 - 324 - 0891 - 91/95). Additional support was provided by Dr. V.B. Kutner, head of the Ion Source Sector.

References

* Permanent address: Institute of Physics, Slovak Academy of Sciences, Dúbravská cesta 9, 842 28 Bratislava, Slovakia.

[1] A.A. Efremov, A.I. Ivanenko, V.B. Kutner, J. Pivarč, and K.D. Tumanov, in *Proceedings of the 3rd European Particle Accelerator Conference (EPAC92)*, Berlin 24 - 28 March, 1992, edited by H. Henke, H. Homeyer and Ch. Petit - Jean Genaz (Fong and Sons Printers Pte. Ltd., Singapore, 1992), Vol. 2, p. 1567.

[2] *Proposal for a Heavy Ion ECR - Source at the PSI - Phylips Cyclotron*, edited by J. Kern and H. Gaggeler (Report PSI - Bericht Nr. 40, Paul Scherrer Institute, Würelingen and Villigen, CH - 5232 Villigen, Switzerland, 1989).

[3] O. Gröbner, in *Proceedings of the CAS CERN Accelerator School General Accelerator Physics*, Gif-sur-Yvette, Paris 3 - 14 September, 1984, edited by P. Bryant and S. Turner (Report CERN 85 - 19, Geneva, 1985), Vol. 2, p. 489.

[4] R. Geller, B. Jacquot, and M. Pontonnier, Rev. Sci. Instr. **56** (8), 1505 (1985).

[5] M. Cavenago, and G. Bisoffi, Nucl. Instr. Meth. in Phys. Res. **A 301**, 9 (1991).

[6] V.E. Golant, J. Theor. Phys. **41** (12), 2492 (1971) in Russian.

[7] F.W. Mayer, in *Proceedings of the 7th International ECR Source Workshop*, Jülich 22 - 23 May,

1986, edited by Hans Beuscher (Jül - Conf. 57, KFA Kernforschungsanlage GmbH, Jülich, 1986) p.11.

[8] S. Deshman, *Nauchnye osnovy vakuumnoj techniky* (Izdatelstvo "MIR", Moskva 1964) in Russian (Translation from the *"Scientific Foundation of Vacuum Technique"*, Second Edition (J. Willey, New York, 1962).

[9] A. Roth, *Vacuum Technology* (North - Holland Publishing Company, Amsterdam - New York - Oxford, 1976).

[10] E.D. Erikson, T.G. Beat, D.D. Berger, and B.A. Frazier, J. Vac. Sci. Technol. **A 2**, 206 (1984).

[10] G. Lee, IEEE Trans. on Nucl. Sc. **NS - 32**, 3806, (1985).

[12] G. Egelmann, M. Genet, and W. Wahl, J. Vac. Sci. Technol. **A 5**, 2337 (1987).

[13] B.A. Trickett, Vacuum **28**, 471 (1978).

[14] J. Pivarč, Jemná mechanika a optika **33** (4), 121 (1988) in Slovak.

[15] F. Doni, C. Boffito, and B. Ferrario, J. Vac. Sci. Technol. **A 4**, 2447 (1986).

[16] M.E. Malinowski, J. Vac. Sci. Technol. **A 3**, 483 (1985).

[17] A. Andritschky, O. Gröbner, A.G. Mathewson, F. Schumann, P. Strubin, and R. Souchet, Vacuum **38**, 933 (1988).

[18] J. Crank, *The Mathematics of Diffusion* (University of Oxford, Oxford, 1975).

[19] J.P. Rajzer, *Fizika gazovogo razrjada* (Nauka, Glavnaja redakcija Fiziko - matematicheskoj literatury, Moskva, 1987), p.130 in Russian.

[20] R. Becker, E.D. Donets, and G.D. Schirkov, Report **E9 - 91 - 382** (Joint Institute for Nuclear Research, Dubna, Russia, 1991).

[21] R.C. Pardo, and P.J. Billquist, Rev. Sci. Instrum. **61**, 239 (1990).

[22] V.B. Kutner, *Private communication,* Dubna, Russia, 1991 (unpublished) in Russian.

[23] R.N. Peacock, J. Vac. Sci. Technol. **17**, 330 (1980).

Received by Publishing Department
on September 6, 1993.